Nanoscale

ROYAL SOCIETY OF CHEMISTRY

COMMUNICATION

View Article Online
View Journal | View Issue

Cite this: *Nanoscale*, 2021, **13**, 10329

Received 16th March 2021,
Accepted 26th April 2021

DOI: 10.1039/d1nr01671g

rsc.li/nanoscale

A general approach to realizing perovskite nanocrystals with insulating metal sulfate shells†

Feng Gao,[a] Jianghua Wu,[b] Yilin Zhao,[a] Tinglu Song,[a] Zhengtao Deng,[c] Peng Wang,[b] Yonggang Wang[d] and Hongbo Li*[a]

The strategy of constructing the core/shell structure is of great importance in emitting semiconductor nanocrystals. However, the coating on soft metal halide perovskite nanocrystals at the single particle level remains a challenge because of the low compatibility between perovskites and common wide-band-gap semiconductors, such as ZnS and CdS. In addition, using these semiconductors as the shell layer requires high reaction temperatures, which often lead to undesirable chemical transformation. Herein we report a general route to passivate the perovskite nanocrystals by insulating metal sulfate shells. The passivating shell is created around the as-synthesized $CsPbBr_3$ perovskite nanocrystals by initiating the reaction between an organic ammonium sulfate and a variety of metal ions in the presence of ligands. This new method allowed for creating insulating metal sulfate shells with controllable thicknesses and without unwanted chemical transformation. Importantly, these novel core/shell-structured nanocrystals show photoluminescence quantum yields near unity, highly suppressed energy transfer in film and suppressed halide exchange in solution.

Introduction

As a newly emerging class of emitting semiconductor materials, cesium lead halide perovskite nanocrystals (NCs) possess unique electronic and optical properties, including narrow emission peaks, widely tunable emission and high photoluminescence quantum yield (PL QY).[1–5] Therefore, perovskite NCs are considered promising candidates for next-generation photovoltaic devices,[6–10] light-emitting diodes,[11–14] photodetectors,[15–17] and lasers.[18–20] However, the intrinsic ionic feature of such materials imposes great challenges on their stability both in colloidal states and in devices.[21–23] To date, many attempts have been made to improve the stability of perovskite NCs. Recently, Li and co-workers proposed a melt crystallization solid-state synthetic strategy for the direct preparation of $CsPbBr_3$ NCs inside a $SrBr_2$ matrix.[24] Kamat and co-workers utilized $PbSO_4$–oleate to cap the $CsPbBr_3$ NCs and $CsPbI_3$ NCs, which successfully improved the stability and suppressed the halide ion exchange.[25] Silica has also been used as a matrix to protect the inorganic perovskite NCs.[26] In addition to these approaches, coating is an alternative and effective way to improve the stability of perovskite NCs. Coating the conventional semiconductor NC core with a shell of a wide-band-gap semiconductor (such as CdS, ZnS) has achieved great success, in terms of improved colloidal stability and PL QY, which has promoted their application in optoelectronic devices.[27–30] Unfortunately, unlike the classical shell coating strategies for metal chalcogenide NCs and metal phosphide NCs, applying the same shell coating strategies in perovskite cores is generally accompanied by undesirable chemical and morphological transformation of the perovskite core because a high reaction temperature approaching 300 °C is often required to guarantee the high-quality coating of ZnS or CdS.[31–33] It is known that metal halide perovskites cannot endure such high temperatures owing to their relatively low formation energy. In addition, cesium lead halide perovskites display highly ionic features and relatively large lattice constants that are incompatible with the wide-band-gap semiconductors. Thus far, very few reports have demonstrated the chemical synthesis of core/shell perovskite NCs at the single particle level.[34–36] Notably, a shell that has completely different elements from the core is helpful to fully retain their unique properties.[37,38] Therefore, it is still rather challenging yet important to develop an ideal shell-coating protocol for the perovskite NCs.

Here we demonstrate a new synthesis strategy for fabricating core/shell perovskite NCs to boost PL QY, improve colloidal

[a]*Experimental Center of Advanced Materials, School of Materials Science and Engineering, Beijing Institute of Technology, 5 Zhongguancun South Street, Beijing 100081, China. E-mail: hongbo.li@bit.edu.cn*
[b]*National Laboratory of Solid State Microstructures, College of Engineering and Applied Sciences and Collaborative Innovation Center of Advanced Microstructures, Nanjing University, Jiangsu 210093, China*
[c]*College of Engineering and Applied Sciences, Nanjing University, Jiangsu 210093, China*
[d]*Center for High Pressure Science and Technology Advanced Re-search, Beijing, 100094, China*

†Electronic supplementary information (ESI) available. See DOI: 10.1039/d1nr01671g

stability and suppress the halide ion exchange reaction in solution. Cesium lead halide $CsPbX_3$ perovskite NCs are intrinsically ionic. Theoretically, a material displaying the same feature should be an ideal candidate for the shell coating layer. Therefore, we selected metal sulfates, a class of ionic insulators, as the shell layer for the core of the perovskite NCs. Our experimental results show that it is possible to achieve a uniform shell of metal sulfate with a controlled shell thickness ranging from 1 up to 3 nm, and the resulting core/shell perovskite NCs display enhanced properties in terms of colloidal stability and PL QY. Following the well-established procedure for achieving a wide-band-gap semiconductor layer under high temperature conditions, we apply mild conditions and develop a general method for the shell coating by adding organic ammonium sulfates and metal ions in the form of organic–metal complex to pre-synthesized perovskite NCs (Scheme 1).

The $CsPbBr_3$ perovskite NCs as the seeds were prepared by injecting cesium oleate (Cs–OA) to react with lead bromide in the presence of oleic acid (OA) and olelylamine (OAm) as the ligands. The reaction temperature was set at 180 °C. Details of the synthesis procedure are provided in the ESI.† The transmission electron microscopy (TEM) image (Fig. 1a) shows an average size of 8.2 nm with a narrow size distribution. Previous works have reported the phenomenon of size increasing for perovskite NCs at room temperature because of the residual unreacted precursors.[39,40] To ensure that the size increasing in the next step was due to the shell coating, rather than self-growth, the $CsPbBr_3$ perovskite NCs were immediately separated from the crude solution by centrifugation, and re-dispersed in a mixture of fresh octadecene and OAm. Furthermore, the reaction temperature was reduced to 75 °C for the shell coating.

As an example, zinc sulfate ($ZnSO_4$) was selected as the shell material for $CsPbBr_3$ NC cores. Bulk $ZnSO_4$ crystallizes in the space group *Pnma* with lattice parameters well compatible with those of orthorhombic $CsPbBr_3$, which facilitates the epitaxial growth of shells onto perovskite NCs. Electron location function (ELF) simulation shows that there is a good match between the (010) facets of $ZnSO_4$ and the (004) facets of $CsPbBr_3$ in terms of lattice constants and the Cs/Zn sublattices (Fig. S1, ESI†). Possible Zn–Br and Cs–O ionic bonding is expected to form at the core/shell interface. The formation of Zn_{Cs} and Cs_{Zn} substitutional defects can suppress the formation of V_{Cs} defects on the core surface, which is generally believed to be responsible for the unfavorable PL quenching. During the shell coating step, the average size gradually increased under the conditions as different amounts of zinc and sulfate precursors were added (Fig. 1b and c). Average size of the $CsPbBr_3/ZnSO_4$ core/shell NCs in Fig. 1b is found to be 11.2 nm in edge length and the shell thickness is estimated to be 1.6 nm. Importantly, the size distribution was not broadened, suggesting that the shell is uniformly coated onto the seeds. Fig. 1c shows that the final $CsPbBr_3/ZnSO_4$ core/shell NCs are still monodisperse; the average size is 14.2 nm, revealing that on average 6 monolayers of $ZnSO_4$ (0.48 nm per monolayer) shell were coated around each core.

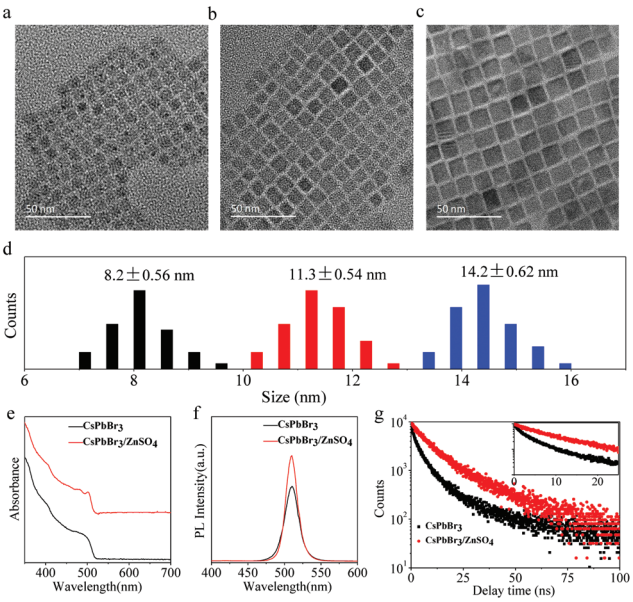

Fig. 1 (a–c) TEM images of perovskite NCs before coating (a) and the resulting core/shell perovskite NCs (b and c). (d) Size distributions of the NCs in (a–c). (e and f) Comparison of the absorption and PL before and after coating. (g) Transient PL spectra of the samples ($CsPbBr_3$ NCs and $CsPbBr_3/ZnSO_4$ NCs) in solution.

To examine the effect of shell coating to the $CsPbBr_3$ core, we recorded the absorption and PL spectra (Fig. 1e and f) of $CsPbBr_3$ NCs and $CsPbBr_3/ZnSO_4$ core/shell NCs. The $CsPbBr_3$ NCs of 8.2 nm show a typical absorption band with no evident peak (estimated at ~504 nm by second-order derivative), and a very narrow PL (full width at half-maximum, FWHM, 20 nm) with the peak position at 515 nm. Common metal sulfates such as $ZnSO_4$, $MgSO_4$ and Rb_2SO_4 are ionic crystals and insulators; therefore, as expected, the absorption spectrum of core/shell sample exhibits a nearly identical profile, suggesting that the shell material does not introduce any new excitonic transitions. Unexpectedly, we found that the absorption band after coating shows a slight yet observable peak at 502 nm, which is due to the elimination of defect states near the edge of the band gap.[41] After the shell coating, the PL peak at 515 nm and the FWHM were retained. The insensitivity of PL peak position to the coated shell was attributed to the insulating nature of

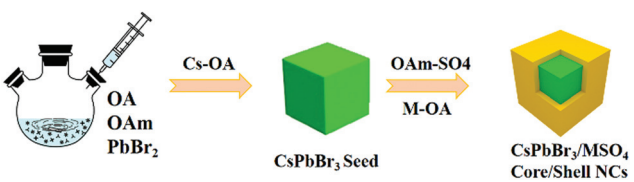

Scheme 1 The schematic illustration of the synthesis procedure of coating metal sulfate shells. The $CsPbBr_3$ perovskite NCs are coated by adding metal oleate (M–OA) and oleylammonium sulfate (OAm–SO_4), yielding the core/shell perovskite NCs.

metal sulfates, which can provide sufficient band gap offsets in terms of both the conduction band and valence band of the $CsPbBr_3$. The insensitivity observed here for this new type of core/shell NCs is distinctly different from that for conventional core/shell NCs.[42,43]

The PL QY of core/shell NCs was improved to nearly unity (95%, from 72% for the bare core), suggesting that the $ZnSO_4$ shell plays a vital role in removing the surface defects that offer a non-recombination pathway. To gain more in-depth insights into the surface defects eliminated by the formation of the core/shell structure, we recorded the time-resolved photoluminescence (TRPL) decay behaviors of $CsPbBr_3$ and $CsPbBr_3/ZnSO_4$ NCs (Fig. 1g). The decay of excitons in the $CsPbBr_3$ NCs displays a nonlinear decay kinetics and a typical average lifetime of 4.4 ns (fitted by a bi-exponential function). This nonlinear feature has been ascribed to the imperfect surface passivation, which is caused by the weak bonding between native ligand pairs and the $CdPbBr_3$.[44–46] After shell coating, the decay characteristic became nearly linear, and the average lifetime was prolonged to 10.7 ns. Importantly, the size of the emitting center is nearly the same according to absorption and PL spectra. As discussed above, the emission essentially comes from the $CsPbBr_3$ seeds. Therefore, the longer average lifetime can be ascribed to the reduced defects due to better passivation offered by the $ZnSO_4$ shell.

To further confirm whether the shell is uniformly coated around the core, we also conducted X-ray photoelectron spectroscopy (XPS), high-resolution STEM and energy-dispersive X-ray spectrometry (EDS) mapping. The surface chemical compositions of the $CsPbBr_3/ZnSO_4$ NCs were characterized by XPS. As shown in Fig. S2,† the wide range XPS spectrum of the coated sample reveals the signals of Cs-3d, Pb-4f, Br-3d, Zn-2p, S-2p and O-1s indicating the presence of all elements involved in the synthesis. Besides, the Zn, S and O peaks display a much higher intensity than the Cs, Pb, and Br peaks, confirming that the surface atoms of the coated sample are dominated by Zn, S and O, which is consistent with the observation of size increase from TEM results. STEM (Fig. 2a) and EDS mapping (Fig. 2b–g) results further confirmed the core/shell hetero-structure. Elemental mapping of perovskite NCs is non-trivial because dramatic ion diffusion was observed under electron beam irradiation, which is consistent with earlier reports.[47] Nevertheless, we observed that the signals of Zn, S and O from the shell are slightly more pronounced than those of Pb, Cs and Br, suggesting the formation of the $ZnSO_4$ shell. The high-resolution STEM result shows a lattice spacing of 0.6 nm, corresponding to the *d*-spacing of the (100) plane of the orthorhombic $CsPbBr_3$. This rules out the possibility of any chemical transformations during the shell coating step. The high-resolution STEM image (Fig. 2h) revealed a distinct boundary between the crystalline $CsPbBr_3$ core and the coating shell, which again supports the formation of the core/shell structure.

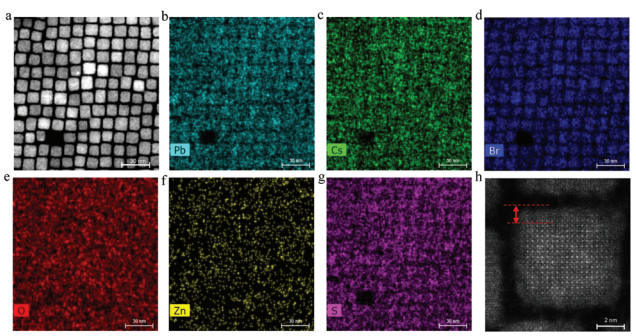

Fig. 2 (a) STEM image, (b–g) EDS maps and (h) high-resolution STEM image of $CsPbBr_3/ZnSO_4$ core/shell NCs.

An important advantage of metal sulfate shell coating is the significant suppression of PL quenching in films. Indeed, PL quenching due to energy transfer in the solid state of perovskite NC films has recently been documented,[48,49] therefore it is worth further investigating the energy transfer in the core/shell perovskite NC film by introducing an insulating metal sulfate shell to $CsPbBr_3$ NCs. Specifically, the insulating shell provides a sufficiently large energy barrier that isolates both the electron and the hole wave-functions from surface defects and deleterious effects of the environment. Furthermore, the thick $ZnSO_4$ shell is conducive to increasing the spatial separation between emitting cores, which is a key parameter for inter-particle energy transfer.

To evaluate the beneficial effect of the insulating shell, we studied close-packed, spin-coated films of the perovskite $CsPbBr_3$ NCs (size of 7.0 nm) without and with a metal sulfate shell. The energy transfer in samples of $CsPbBr_3/ZnSO_4$ core/shell NCs was expected to be considerably suppressed compared with that for uncoated samples because of the presence of the insulating shell. As expected, we confirmed the PL quenching in film by observing a small yet measurable red-shift (*ca.* 1 nm), as shown in Fig. 3a. This is a clear indication of exciton migration, as has been observed in previous studies.[50] In contrast, for the films of metal–sulfate-coated core/shell NCs, the PL profile is indistinguishable from that of the solution sample (Fig. 3b), which is a clear indication of the suppressed energy transfer. This beneficial property due to the insulating shell is further confirmed by assessing the PL efficiencies measured by an integrating sphere method. The PL QY of the perovskite $CsPbBr_3$ NCs film (50%) is quenched by ~31% in the solid state compared to NCs in solution. In contrast, the PL QY of films of $ZnSO_4$-coated core/shell NCs is 92%, only slightly lower than that of NCs in solution (95%).

The TRPL curves recorded from the dilute solution and the dense solid film of $CsPbBr_3$ NCs give the average lifetimes of 4.0 ns and 2.5 ns, respectively (Fig. 3c, fitted by a bi-exponential function). The average lifetime of energy transfer is calculated to be 6.7 ns, and the energy transfer efficiency is 37.5% (for details of calculation, please see the ESI†). In contrast, the PL decay characteristic of $CsPbBr_3/ZnSO_4$ core/shell NCs in solid film is nearly the same as that in solution. The TRPL curves recorded from the dilute solution and the solid film give the average lifetime of 6.7 nm and 6.3 ns, respectively (Fig. 3d). The average lifetime of energy transfer is calculated

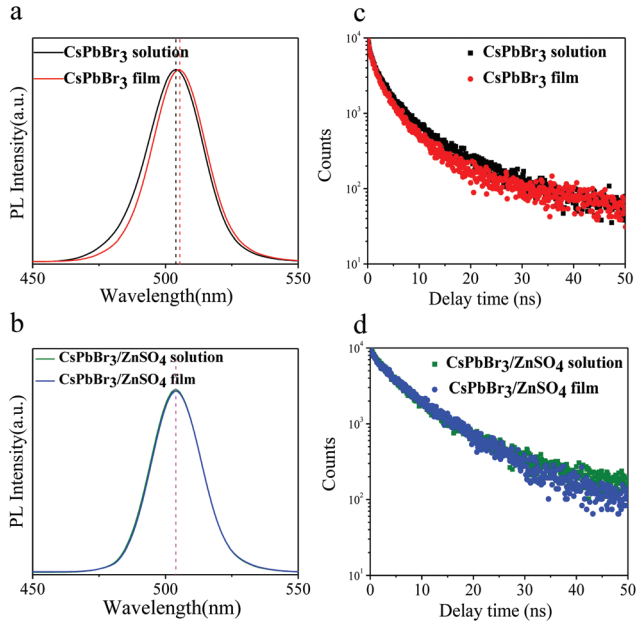

Fig. 3 PL and decay curves recorded from film *vs.* solution samples of $ZnSO_4$-coated (shell thickness, 3 nm) and uncoated perovskite NCs. (a) PL spectra of uncoated NCs in hexane (black) and spin-coated film (red). (b) PL spectra of $ZnSO_4$ coated core/shell NCs in hexane (green) and spin-coated film (blue). The ~1 nm redshift of the PL peak of the film *vs.* solution sample in the case of uncoated g-NCs is a signature of energy transfer, whereas, this redshift is absent for $ZnSO_4$-coated core/shell NCs, indicating a strong suppression of energy transfer. (c and d) Transient PL spectra of the coated and uncoated samples in solution and in film.

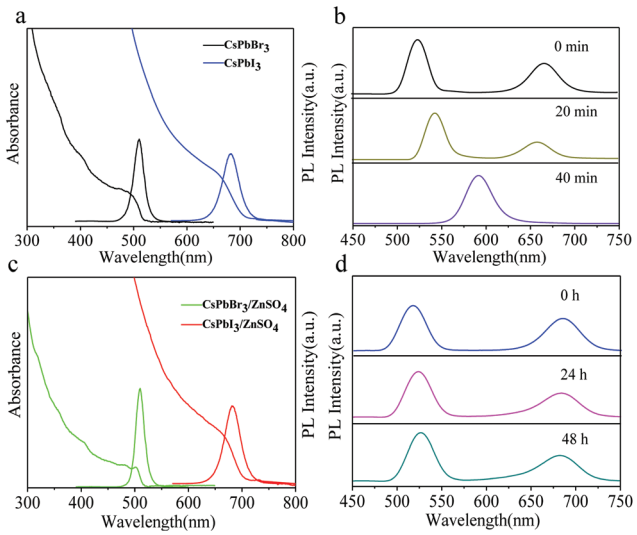

Fig. 4 Suppression of inter-particle halide exchange (a) optical absorption and PL spectra of $CsPbBr_3$ and $CsPbI_3$ NCs. (b) PL spectra obtained at different reaction times after mixing the solution of $CsPbBr_3$ and $CsPbI_3$. (c) Optical absorption and PL spectra of $CsPbBr_3/ZnSO_4$ and $CsPbI_3/ZnSO_4$ core/shell NCs. (d) PL spectra obtained at different reaction times after mixing the solution of $CsPbBr_3/ZnSO_4$ and $CsPbI_3/ZnSO_4$.

to be 106 ns and the energy transfer efficiency is only 5.9%, suggesting a very strong suppression of energy transfer in film.

An additional important benefit of the metal sulfate shell is the significantly suppressed halide exchange and the improved long-term photo stability. To verify these points, we first performed the halide exchange reaction in solution using $CsPbX_3$ (X = Br, I) NCs and $CsPbX_3/ZnSO_4$ core/shell NCs separately. Further experimental details on testing the halide exchange in these core/shell NCs are provided in the ESI.† As shown in Fig. 4a and b, the halide exchange reaction between $CsPbBr_3$ NCs and $CsPbI_3$ NCs was initiated upon mixing, and was completed in 40 min, as indicated by a rapid evolution of the PL profile, which is consistent with previously reported results.[51–54] In contrast, the halide exchange reaction between the coated as-prepared $CsPbBr_3/ZnSO_4$ NCs and $CsPbI_3/ZnSO_4$ was strongly suppressed (Fig. 4c and d). The PL profile could remain stable for up to 48 h. Although we noticed that the PL profile corresponding to $CsPbI_3$ NCs gradually became asymmetric, (suggesting that halide ion exchanges might have taken place to some extent), the observed effects are very distinct from those for the mixing bare $CsPbBr_3$ NCs and $CsPbI_3$ NCs (Fig. 4b). Therefore, these results confirm the suppression of halide exchange after coating the $ZnSO_4$ shell.

Furthermore, we compared the stability of $CsPbBr_3$ NCs and $CsPbBr_3/ZnSO_4$ core/shell NCs in air (Fig. S3†). We found that the PL QY of the $CsPbBr_3$ NCs solution was dramatically decreased (from 72% to 53.1%) within seven days, consistent with previously reported results. For the $CsPbBr_3/ZnSO_4$ core/shell NCs, as expected, the PL QY exhibited a slight drop (by 3.6%), indicating improved PL stability in air after shell coating (Fig. S3†).

By changing the metal ions, we can achieve similar coating results in terms of controlling the shell thickness, retained size distribution, enhanced PL efficiency. As shown in Fig. S4 and S5 in the ESI,† we obtained core/shell NCs with different metal sulfates as the shells, including $MgSO_4$ and Rb_2SO_4. We observed results similar to those with the $ZnSO_4$ shell, such as size increase, PL enhancement. The TEM images of $CsPbBr_3/MgSO_4$ and $CsPbBr_3/Rb_2SO_4$ show an average size of 13.6 nm and 13.5 nm, respectively. EDS results reveals the presence of corresponding elements in the final core/shell NCs. The signal of each elements, particularly Mg, Rb and S from the metal sulfates, is found in the core/shell samples, implying that our approach here provides a general way to coat perovskite NCs with metal sulfates.

Conclusions

In summary, we developed a general protocol to prepare core/shell perovskite NCs with an insulating metal sulfate shell. We found that in our new method the formation of the metal sulfate shell does not alter the size and size distribution of the original seeds, and at the same time, the insulating shell can remove potential defects at the surface. This new shell layer is uniformly coated onto the NCs at a single particle level, which

guarantees the good confinement of excitons in solution and in the solid state. The obtained core/shell NCs display PL QY near unity, and much improved stability. Importantly, the metal sulfate shells with a thickness of 3 nm can effectively suppress the energy transfer in dense film and the halide exchange in solution.

Author contributions

H. L. proposed the idea, designed the experiments and wrote the manuscript, F. G. and Y. Z. conducted the experiments and optical measurement. J. W. and P. W. performed the elemental mapping analysis. Z. D. and Y. W. optimized the scheme and figures. F. G. and J. W. contributed equally to this work.

Conflicts of interest

There are no conflicts to declare.

Acknowledgements

We gratefully acknowledge the financial support from the National Natural Science Foundation of China (Grant No. 21701015, 22005034, 22075129 and 21811530054).

Notes and references

1 L. Protesescu, S. Yakunin, M. I. Bodnarchuk, F. Krieg, R. Caputo, C. H. Hendon, R. X. Yang, A. Walsh and M. V. Kovalenko, *Nano Lett.*, 2015, **15**, 3692–3696.
2 M. V. Kovalenko, L. Protesescu and M. I. Bodnarchuk, *Science*, 2017, **358**, 745–750.
3 L. N. Quan, B. P. Rand, R. H. Friend, S. G. Mhaisalkar, T.-W. Lee and E. H. Sargent, *Chem. Rev.*, 2019, **119**, 7444–7477.
4 H. Utzat, W. Sun, A. E. K. Kaplan, F. Krieg, M. Ginterseder, B. Spokoyny, N. D. Klein, K. E. Shulenberger, C. F. Perkinson, M. V. Kovalenko and M. G. Bawendi, *Science*, 2019, **363**, 1068–1072.
5 C. R. Kagan, *Chem. Soc. Rev.*, 2019, **48**, 1626–1641.
6 Q. A. Akkerman, M. Gandini, F. Di Stasio, P. Rastogi, F. Palazon, G. Bertoni, J. M. Ball, M. Prato, A. Petrozza and L. Manna, *Nat. Energy*, 2016, **2**, 16194.
7 A. Swarnkar, A. R. Marshall, E. M. Sanehira, B. D. Chernomordik, D. T. Moore, J. A. Christians, T. Chakrabarti and J. M. Luther, *Science*, 2016, **354**, 92–95.
8 X. Luo, T. Ding, X. Liu, Y. Liu and K. Wu, *Nano Lett.*, 2019, **19**, 338–341.
9 X. Zheng, J. Troughton, N. Gasparini, Y. Lin, M. Wei, Y. Hou, J. Liu, K. Song, Z. Chen, C. Yang, B. Turedi, A. Y. Alsalloum, J. Pan, J. Chen, A. A. Zhumekenov, T. D. Anthopoulos, Y. Han, D. Baran, O. F. Mohammed, E. H. Sargent and O. M. Bakr, *Joule*, 2019, **3**, 1963–1976.
10 J. Zhang, G. Hodes, Z. Jin and S. F. Liu, *Angew. Chem., Int. Ed.*, 2019, **58**, 15596–15618.
11 J. Song, J. Li, X. Li, L. Xu, Y. Dong and H. Zeng, *Adv. Mater.*, 2015, **27**, 7162–7167.
12 Z. W. Zhuang, C. D. Peng, G. Y. Zhang, H. M. Yang, J. L. Yin and H. H. Fei, *Angew. Chem., Int. Ed.*, 2017, **56**, 14411–14416.
13 Y. Wei, Z. Cheng and J. Lin, *Chem. Soc. Rev.*, 2019, **48**, 310–350.
14 B. B. Zhang, S. Yuan, J. P. Ma, Y. Zhou, J. Hou, X. Chen, W. Zheng, H. Shen, X. C. Wang, B. Sun, O. M. Bakr, L. S. Liao and H. T. Sun, *J. Am. Chem. Soc.*, 2019, **141**, 15423–15432.
15 Q. Chen, J. Wu, X. Ou, B. Huang, J. Almutlaq, A. A. Zhumekenov, X. Guan, S. Han, L. Liang, Z. Yi, J. Li, X. Xie, Y. Wang, Y. Li, D. Fan, D. B. L. Teh, A. H. All, O. F. Mohammed, O. M. Bakr, T. Wu, M. Bettinelli, H. Yang, W. Huang and X. Liu, *Nature*, 2018, **561**, 88–93.
16 C. Bi, S. V. Kershaw, A. L. Rogach and J. Tian, *Adv. Funct. Mater.*, 2019, **29**, 1902446.
17 M. Gandini, I. Villa, M. Beretta, C. Gotti, M. Imran, F. Carulli, E. Fantuzzi, M. Sassi, M. Zaffalon, C. Brofferio, L. Manna, L. Beverina, A. Vedda, M. Fasoli, L. Gironi and S. Brovelli, *Nat. Nanotechnol.*, 2020, **15**, 462–468.
18 G. Raino, M. A. Becker, M. I. Bodnarchuk, R. F. Mahrt, M. V. Kovalenko and T. Stoferle, *Nature*, 2018, **563**, 671–675.
19 S. Wang, J. Yu, M. Zhang, D. Chen, C. Li, R. Chen, G. Jia, A. L. Rogach and X. Yang, *Nano Lett.*, 2019, **19**, 6315–6322.
20 D. Vila-Liarte, M. W. Feil, A. Manzi, J. L. Garcia-Pomar, H. Huang, M. Doblinger, L. M. Liz-Marzan, J. Feldmann, L. Polavarapu and A. Mihi, *Angew. Chem., Int. Ed.*, 2020, **59**, 17750–17756.
21 X. He, Y. Qiu and S. Yang, *Adv. Mater.*, 2017, **29**, 1700775.
22 Z. Li, L. Kong, S. Huang and L. Li, *Angew. Chem., Int. Ed.*, 2017, **56**, 8134–8138.
23 G. Almeida, I. Infante and L. Manna, *Science*, 2019, **364**, 833–834.
24 B. Wang, C. Zhang, W. Zheng, Q. Zhang, Q. Wan, L. Kong and L. Li, *Chem. Commun.*, 2020, **56**, 11291–11294.
25 V. K. Ravi, R. A. Scheidt, A. Nag, M. Kuno and P. V. Kamat, *ACS Energy Lett.*, 2018, **3**, 1049–1055.
26 Y. Liu, F. Li, Q. Liu and Z. Xia, *Chem. Mater.*, 2018, **30**, 6922–6929.
27 M. A. Hines and P. Guyot-Sionnest, *J. Phys. Chem.*, 1996, **100**, 468–471.
28 J. J. Li, Y. A. Wang, W. Z. Guo, J. C. Keay, T. D. Mishima, M. B. Johnson and X. G. Peng, *J. Am. Chem. Soc.*, 2003, **125**, 12567–12575.
29 P. Reiss, M. Protiere and L. Li, *Small*, 2009, **5**, 154–168.
30 T. Kim, K. H. Kim, S. Kim, S. M. Choi, H. Jang, H. K. Seo, H. Lee, D. Y. Chung and E. Jang, *Nature*, 2020, **586**, 385–389.
31 B. Jin, N. Zuo, Z. Y. Hu, W. Cui, R. Wang, G. Van Tendeloo, X. Zhou and T. Zhai, *Adv. Funct. Mater.*, 2020, **30**, 2006166.

32 V. K. Ravi, S. Saikia, S. Yadav, V. V. Nawale and A. Nag, *ACS Energy Lett.*, 2020, **5**, 1794–1796.
33 J. Shi, W. Ge, J. Zhu, M. Saruyama and T. Teranishi, *ACS Appl. Nano Mater.*, 2020, **3**, 7563–7571.
34 B. Qiao, P. Song, J. Cao, S. Zhao, Z. Shen, G. Di, Z. Liang, Z. Xu, D. Song and X. Xu, *Nanotechnology*, 2017, **28**, 445602.
35 C. Jia, H. Li, X. Meng and H. Li, *Chem. Commun.*, 2018, **54**, 6300–6303.
36 X. Zhang, W. Yin, W. Zheng and A. L. Rogach, *ACS Energy Lett.*, 2020, **5**, 2927–2934.
37 A. Loiudice, M. Strach, S. Saris, D. Chernyshov and R. Buonsanti, *J. Am. Chem. Soc.*, 2019, **141**, 8254–8263.
38 Q. Kong, A. Obliger, M. Lai, M. Gao, D. T. Limmer and P. Yang, *Nano Lett.*, 2020, **20**, 8151–8156.
39 M. Imran, V. Caligiuri, M. Wang, L. Goldoni, M. Prato, R. Krahne, L. De Trizio and L. Manna, *J. Am. Chem. Soc.*, 2018, **140**, 2656–2664.
40 A. Dutta, R. K. Behera, P. Pal, S. Baitalik and N. Pradhan, *Angew. Chem., Int. Ed.*, 2019, **58**, 5552–5556.
41 H. L. B. Bostrom, J. Bruckmoser and A. L. Goodwin, *J. Am. Chem. Soc.*, 2019, **141**, 17978–17982.
42 O. Chen, J. Zhao, V. P. Chauhan, J. Cui, C. Wong, D. K. Harris, H. Wei, H.-S. Han, D. Fukumura, R. K. Jain and M. G. Bawendi, *Nat. Mater.*, 2013, **12**, 445–451.
43 Y. H. Won, O. Cho, T. Kim, D. Y. Chung, T. Kim, H. Chung, H. Jang, J. Lee, D. Kim and E. Jang, *Nature*, 2019, **575**, 634–638.
44 A. B. Wong, Y. Bekenstein, J. Kang, C. S. Kley, D. Kim, N. A. Gibson, D. Zhang, Y. Yu, S. R. Leone, L. W. Wang, A. P. Alivisatos and P. Yang, *Nano Lett.*, 2018, **18**, 2060–2066.
45 D. P. Nenon, K. Pressler, J. Kang, B. A. Koscher, J. H. Olshansky, W. T. Osowiecki, M. A. Koc, L.-W. Wang and A. P. Alivisatos, *J. Am. Chem. Soc.*, 2018, **140**, 17760–17772.
46 J. Pan, Y. Shang, J. Yin, M. De Bastiani, W. Peng, I. Dursun, L. Sinatra, A. M. El-Zohry, M. N. Hedhili, A.-H. Emwas, O. F. Mohammed, Z. Ning and O. M. Bakr, *J. Am. Chem. Soc.*, 2018, **140**, 562–565.
47 J. B. Hoffman, A. L. Schleper and P. V. Kamat, *J. Am. Chem. Soc.*, 2016, **138**, 8603–8611.
48 L. Protesescu, S. Yakunin, M. I. Bodnarchuk, F. Bertolotti, N. Masciocchi, A. Guagliardi and M. V. Kovalenko, *J. Am. Chem. Soc.*, 2016, **138**, 14202–14205.
49 C. J. Tong, L. Li, L. M. Liu and O. V. Prezhdo, *J. Am. Chem. Soc.*, 2020, **142**, 3060–3068.
50 H. Moon, C. Lee, W. Lee, J. Kim and H. Chae, *Adv. Mater.*, 2019, **31**, 1804294.
51 Q. A. Akkerman, V. D'Innocenzo, S. Accornero, A. Scarpellini, A. Petrozza, M. Prato and L. Manna, *J. Am. Chem. Soc.*, 2015, **137**, 10276–10281.
52 G. Nedelcu, L. Protesescu, S. Yakunin, M. I. Bodnarchuk, M. J. Grotevent and M. V. Kovalenko, *Nano Lett.*, 2015, **15**, 5635–5640.
53 Q. A. Akkerman, E. Bladt, U. Petralanda, Z. Dang, E. Sartori, D. Baranov, A. L. Abdelhady, I. Infante, S. Bals and L. Manna, *Chem. Mater.*, 2019, **31**, 2182–2190.
54 C. Jia, H. Li, L. Tan, X. Meng, J. Gao and H. Li, *Nanoscale*, 2019, **11**, 3123–3128.